Cross compression of light bullets by two-color cofilamentation

Pierre Béjot,[1,*] Jérome Kasparian,[1,2] and Jean-Pierre Wolf[1]
[1]*GAP-Biophotonics, Université de Genève, 20 rue de l'Ecole de Médecine, 1211 Geneva 4, Switzerland*
[2]*Université Lyon 1, CNRS, LASIM UMR 5579, bâtiment A. Kastler, 43 Boulevard du 11 novembre 1918, F-69622 Villeurbanne Cedex, France*
(Received 14 April 2008; published 2 October 2008)

The cofilamentation of two ultrashort laser pulses at 800 and 400 nm in argon is numerically shown to counteract their temporal splitting. The output pulses are as short as 15 and 6.5 fs, respectively, without any postprocess compression or stringent alignment. The simultaneous generation of two sub-millijoule (160 and 15 μJ, respectively) sub-six-cycle pulses at ω and 2ω is of particular interest for attosecond science.

DOI: 10.1103/PhysRevA.78.043804 PACS number(s): 42.65.Tg

Increasing interest has recently been devoted to the generation of single attosecond pulses, because they allow phenomena such as coherent molecular dynamics or Rydberg orbital motion to be probed with attosecond time resolution [1]. However, the generation of attosecond pulses requires few- or even single-cycle driving pulses, causing in turn strong attention to few-cycle pulse (FCP) generation [2–5].

Self-guided filaments induced by ultrashort laser pulses in gases [6–9] provide an efficient way to produce such FCPs. A first approach consists in stopping the filamentation by a gas pressure gradient, before pulse splitting occurs. But this approach requires a complex gas cell design and a careful control of the longitudinal location of filamentation [10]. Alternatively, filaments can generate a broad spectrum by self-phase-modulation (SPM). This continuum is then temporally compressed by chirped mirrors or a pulse shaper [11]. This recompression stage requires both careful design and alignment. Moreover, the spectral width of the continuum is critical.

The use of a dual-color pulse can improve this bandwidth. Recently, numerical simulations suggested that a weak seed pulse at frequency ω_s copropagating with a filament at ω_0 can generate an ultrabroad continuum at $\omega_{\mathrm{FWM}}=2\omega_0-\omega_s$ through four-wave mixing (FWM) and produce a FCP at 545 nm without any postcompression stage [12]. The induced light bullet can then propagate over about 0.25 m, much farther than expected by consideration of the group-velocity dispersion. The interplay between self-phase-modulation and cross-phase modulation (XPM) between two pulses at different wavelengths (e.g., 400 and 800 nm) copropagating in a gas-filled hollow-core fiber [13,14] also generates an ultrabroad continuum in the visible region. The same SPM-XPM interplay was also demonstrated in the case of copropagating filaments, resulting in an ultrabroad continuum in either the deep uv [3,15] or the far infrared [16]. However, the output bandwidth and time duration of the initial pulses has not been characterized so far.

In addition to enhancing the spectral broadening, the use of a two-color pair of ultrashort pulses at frequencies ω and 2ω breaks the temporal symmetry of the electric field. Therefore, the emission of attosecond pulses in the cutoff photon energy region takes place every full cycle instead of every half cycle and the duration requirements for the driving pulse are reduced by a factor of 2, allowing the use of multicycle pulses [17–22].

Hence, the simultaneous generation of a two-color pair of ultrabroadband pulses at both ω and 2ω would help both stages of the attosecond pulse generation: the generation of the FCP and the subsequent production of single attosecond pulses in the higher harmonics. In this paper, we show numerically that the cofilamentation of two laser pulses at $\lambda_{\mathbf{R}}=800$ nm and $\lambda_{\mathbf{B}}=400$ nm in argon indeed generates a pair of intense, sub-six-cycle pulses in a two-color field, meeting the requirements for attosecond pulse generation. Moreover, contrary to existing experimental schemes, this two-color dual pulse is obtained without any temporal postcompression stage or complex gas cell design, leading the way to a practical experimental implementation.

We consider two collinearly polarized incident electric fields at $\lambda_{\mathbf{B}}$ (labeled **B**) and $\lambda_{\mathbf{R}}$ (**R**) with cylindrical symmetry around the propagation axis z. The scalar envelopes are assumed to vary slowly in time and along z. The two fields are coupled by XPM only: Four-wave mixing effects such as $2\omega_{\mathbf{B}}\pm\omega_{\mathbf{R}}$, $2\omega_{\mathbf{R}}\pm\omega_{\mathbf{B}}$ are not taken into account in this discussion because, due to the short coherence length (28 μm to 2.8 mm, depending on the considered wavelength set, i.e., much shorter than the typical 2.5 cm length of the filaments considered in this work), they induce a negligible depletion of the incident pulses. It should also be noted that the FWM efficiency is kept very low (10^3 times lower than the **R** pulse intensity) by the short associated coherence length [25]. Higher-order processes are also neglected. The two scalar envelopes evolve according to the coupled propagation equations (1) and (2) directly derived from the nonlinear unidirectional pulse propagation equation [23] for two copropagating pulses [24]:

$$\partial_z\varepsilon_{\mathbf{B}}=\frac{i}{2k_{\mathbf{B}}}\Delta_\perp^2\varepsilon_{\mathbf{B}}-i\frac{k''_{\mathbf{B}}}{2}\partial_t^2\varepsilon_{\mathbf{B}}-i\Delta_{1/v}\partial_t\varepsilon_{\mathbf{B}}+\frac{ik_{\mathbf{B}}}{n_{\mathbf{B}}}(n_{2_{\mathbf{B}}}|\varepsilon_{\mathbf{B}}|^2+n_{\mathrm{cross}}|\varepsilon_{\mathbf{R}}|^2)\varepsilon_{\mathbf{B}}-\frac{ik_{\mathbf{B}}}{2n_{\mathbf{B}}^2\rho_{c_{\mathbf{B}}}}\rho\varepsilon_{\mathbf{B}}-\frac{1}{2}\sigma_{\mathbf{B}}\rho\varepsilon_{\mathbf{B}}-\frac{\beta_{\mathbf{B}}^{K_{\mathbf{B}}}}{2}|\varepsilon_{\mathbf{B}}|^{2K_{\mathbf{B}}-2}\varepsilon_{\mathbf{B}},\quad(1)$$

*pierre.bejot@unige.ch

TABLE I. Input parameters of the simulations. The difference in the focal length between **R** ad **B** is caused by the longitudinal chromatic aberration of the lens.

	$\lambda_{\mathbf{B}}=400$ nm	$\lambda_{\mathbf{R}}=800$ nm
Energy (mJ)	0.2	1
Δt_{FWHM} (fs)	30	30
σ_r (mm)	6	6
Chirp (fs^2)	0	0
f (m)	1	1.04
Initial delay (fs)	0	0
Pressure (bar)	1	1

$$\partial_z \varepsilon_{\mathbf{R}} = \frac{i}{2k_{\mathbf{R}}}\Delta_\perp^2 \varepsilon_{\mathbf{R}} - i\frac{k''_{\mathbf{R}}}{2}\partial_t^2 \varepsilon_{\mathbf{R}} + \frac{ik_{\mathbf{R}}}{n_{\mathbf{R}}}(n_{2_{\mathbf{R}}}|\varepsilon_{\mathbf{R}}|^2 + n_{\mathrm{cross}}|\varepsilon_{\mathbf{B}}|^2)\varepsilon_{\mathbf{R}} - \frac{ik_{\mathbf{R}}}{2n_{\mathbf{R}}^2\rho_{c_{\mathbf{R}}}}\rho\varepsilon_{\mathbf{R}} - \frac{1}{2}\sigma_{\mathbf{R}}\rho\varepsilon_{\mathbf{R}} - \frac{\beta^{K_{\mathbf{R}}}_{\mathbf{R}}}{2}|\varepsilon_{\mathbf{R}}|^{2K_{\mathbf{R}}-2}\varepsilon_{\mathbf{R}}, \quad (2)$$

where t refers to the retarded time in the reference frame of **R** and the notations are as described in [25]. In Eq. (1), $\Delta_{1/v}=\frac{1}{v_{g_{\mathbf{B}}}}-\frac{1}{v_{g_{\mathbf{R}}}}$ is the walkoff constant between **R** and **B**. The plasma density ρ is coupled to both electric fields through:

$$\partial_t \rho = \left(\sum_{l=\mathbf{B},\mathbf{R}} \sigma_{K_l}|\varepsilon_l|^{2K_l}\right)\left(1-\frac{\rho}{\rho_{\mathrm{at}}}\right) + \frac{1}{U}\sum_{l=\mathbf{B},\mathbf{R}} \sigma_l \rho|\varepsilon_l|^2 - \alpha\rho^2, \quad (3)$$

where α is the recombination time constant. The values of the physical parameters are similar to those of [25]. The input electric field envelopes are modeled in focused geometry by two Gaussian profiles. Both the linear chirp of the pulses and their initial delay [which is positive when **R** reaches the focal region ($z=1m$) before **B**] are set in the frequency space.

We integrated Eqs. (1) and (2) with a Fourier split-step scheme. The linear terms (diffraction and dispersion) are computed in the Fourier space over a half step in a fully implicit scheme [26]. The nonlinear terms are directly computed in the physical space over a second half step using a Runge-Kutta procedure. Equation (3) was integrated by a Euler scheme. We used a fixed 8192-point temporal grid, providing a resolution of 0.25 fs, and an adaptative grid in both the transverse and z dimensions [27], with a transverse resolution down to 1.5 μm where filamentation occurs. The simulation input parameters match those of the experiments described in [25], as summarized in Table I.

To precisely identify the contribution of cofilamentation, we compared the results of numerical simulations of the independent filamentation of both **B** and **R** with the case where the two pulses copropagate, with the same initial conditions. Figure 1 displays the effect of cofilamentation on both the quadratic radius and the intensity in the center of the beams. While **R** is little affected by the cofilamentation in the considered conditions, **B** is refocused twice by cross Kerr focusing. In this process, the photon bath [28,29] of **R** significantly contributes, through a $\chi^{(3)}$ process, to the refocusing of the copropagating **B** pulse. In contrast to **B**, **R** is moderately affected by the cofilamentation. This is due to the fact that the **B** transverse dimension is larger than that of **R** throughout almost the whole propagation (typically 100 vs 25 μm), so that the nonlinear cross effects averaged over the whole **R** cross section remain small. The clamped intensity of both pulses is almost unaffected by cofilamentation and amounts to 11×10^{13} W cm^{-2} for **B** and 6×10^{13} W cm^{-2} for **R** over a few centimeters.

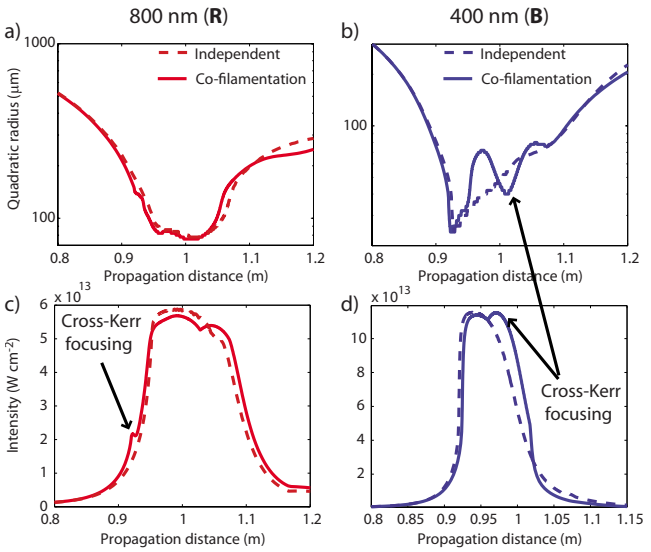

FIG. 1. (Color online) Quadratic radii of 800 (a) and 400 (b) nm pulses as a function of propagation distance for both stand-alone propagation and cofilamentation. When the two pulses copropagate, a second focusing cycle is observed at $z=102$ cm. Correspondingly, the intensity of 800 (c) [400 (d)] nm increases at $z=0.93$ (1) m as B (R) experiences filamentation due to the cross-Kerr-focusing.

As shown in Fig. 2, the cofilamentation also strongly influences the temporal shape of **B**. The independent propaga-

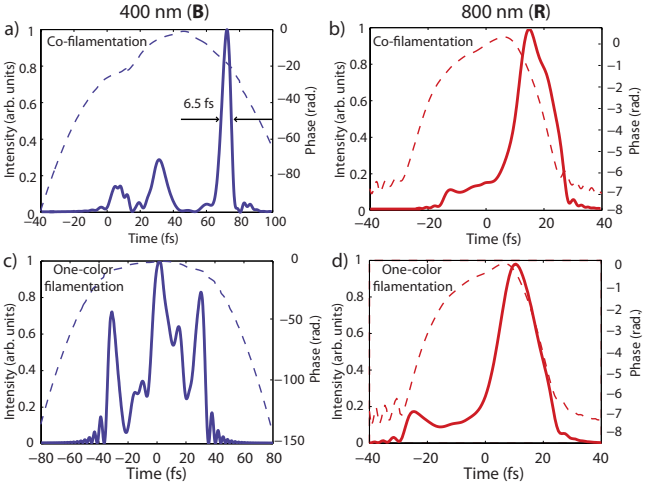

FIG. 2. (Color online) Temporal intensity (solid line) and phase (dashed line) of the 400 (a) and 800 (b) nm pulses after 150 cm propagation, in the case of cofilamentation. Independent propagation is displayed in (c) and (d).

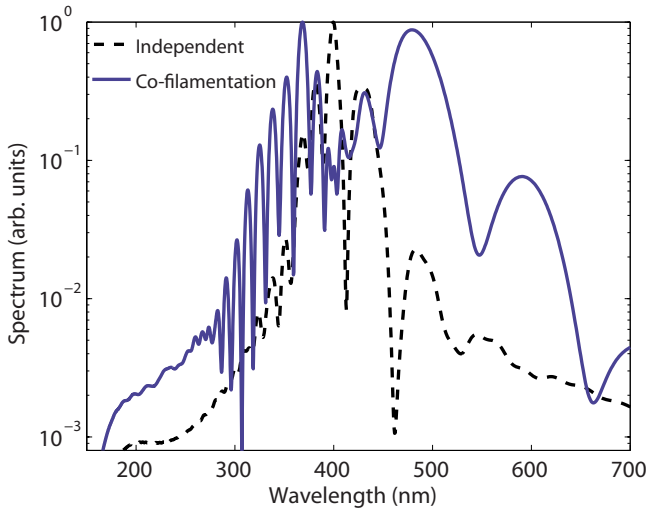

FIG. 3. (Color online) Spectrum around 400 nm. Cofilamentation drastically enhances the spectral broadening through XPM.

tion of **B** gives rise to multiple pulse splitting, resulting in a series of sharp spikes spanning over 100 fs, which would fully prevent single attosecond pulse generation. In contrast, cross Kerr focusing, as well as defocusing and absorption of each pulse by the plasma generated by the other one, partially blocks pulse splitting, generating a 6.5 fs short pulse (4.9 cycles) with little quadratic phase dependency. In the high-intensity temporal region, the phase exhibits an almost linear temporal dependency which indicates a central frequency shift of **B** (the negative slope indicates a central frequency blueshift as can be noticed in Fig. 3). In addition to this slight blueshift, the spectrum of the continuum is greatly broadened as compared with the case of the stand-alone **B** filament (Fig. 3). As in the case of the spatial domain, cofilamentation affects **R** marginally, although it typically reduces the pedestal intensity by a factor of 2 and increases the contrast ratio between the almost FCP (15 fs, i.e., 5.6 cycles) fluence and its pedestal by 2.5.

The space-time plots of Fig. 4 give more insight into the cofilamentation spatiotemporal dynamics. The drastic reduction of pulse splitting as well as the cross Kerr focusing appear clearly. After **B** has experienced multiple pulse splitting, the **R**-induced plasma diffracts and absorbs all the **B** spikes, which temporally occur after **R**. Simultaneously, the (cross) Kerr effect focuses both the **B** and **R** energy reservoirs located around the filaments. Moreover, the effect of cofilamentation on **R** can be seen in Fig. 4(b) at the distance $z=94$ cm, where the plasma generated by **B** defocuses the trailing edge of **R**. Without any postcompression, **R** is composed of only 5.6 cycles (15 fs), while **B** contains about 4.9 cycles (6.5 fs) at $z=150$ cm with a contrast 3.5, 50 cm after the filamentation process. At this distance, **R** (**B**) intensity is as high as 1 (0.3) TW cm^{-2} corresponding to a bullet energy of 160 (13) μJ transversely integrated over 2 mm and disregarding the pedestal. Moreover, the extremely short FWHM time duration of the two light bullets remains stable over more than 20 cm, as expected for temporal solitonlike structures. It may be noted that the above results were recorded in the center of the beam, although the two pulses are

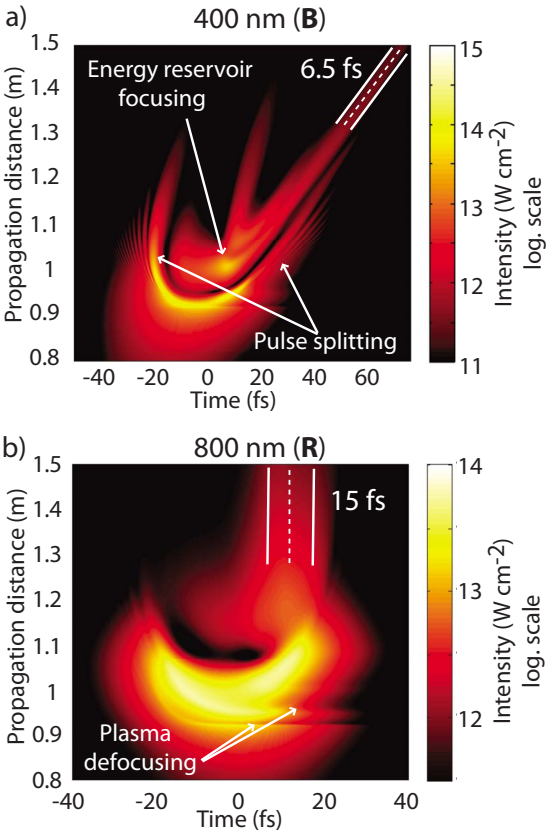

FIG. 4. (Color online) Temporal shape of **B** (a) and **R** (b) as a function of the distance when the two pulses copropagate. The durations of the two pulses [full width at half maximum (FWHM)] remain stable over more than 20 cm from $z=1.3$ to 1.5 m. Note that the walkoff between the two pulses delays **B** in the **R** frame.

transversely inhomogeneous. However, real experiments tackle such inhomogeneities and select the shortest and spectrally broadest regions of the beam by selecting the center of the beam using a pinhole. Therefore, we expect that our calculations are representative of future experiments, which could greatly benefit from the self-aligned character of the proposed technique, as well as the fact that it requires no postcompression. Such advantages, together with its reasonable energy conversion efficiency, make our approach experimentally very attractive as compared with techniques providing a higher yield, but at the cost of more elaborate

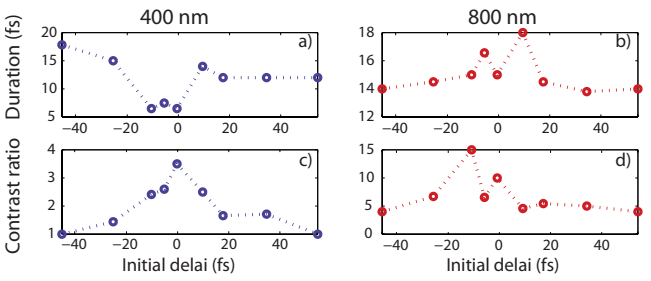

FIG. 5. (Color online) **B** (a) and **R** (b) FWHM duration and contrast ratio (c), (d) after the cofilamentation ($z=150$ cm). Positive delays correspond to the situation where **R** reaches the focal region ($z=1$ m) before **B**.

setups such as hollow waveguides and chirp mirror recompression [30].

The time delay between the pulses, and hence their temporal overlap in the interaction region, critically influences their cofilamentation, and in particular the FWHM duration and the contrast ration of the two copropagating pulses (Fig. 5). While an adequate delay almost inhibits the pulse splitting of the **B** pulse, a detuned delay may have the opposite effect, resulting in a comb of sharp peaks. While the **R** duration is less sensitive to the delay, a perfect overlap yields a threefold increase of the contrast ratio of **R**. Other parameters, like the relative intensities of the two pulses, their wavelength, or the focal length they encounter, are also expected to influence cofilamentation. For example, although such development is beyond the scope of this work, we expect that it would be possible to better compress the **R** pulse by adjusting the relative location of the focus of **R** and **B**.

As a conclusion, we have numerically demonstrated a method to simultaneously generate two sub-six-cycle pulses with subjoule energy. The cross Kerr focusing governing cofilamentation drastically reduces the pulse splitting, resulting in almost few-cycle pulses at both ω and 2ω, which could act as a pair of driving pulses for attosecond pulse generation. The fairly good energy conversion efficiency of this self-aligned and self-recompressed method makes it attractive for practical experiments.

This work was supported by the Swiss NSF (Contracts No. 200021-111688 and No. 200021-116198 and R'equip program), and the Swiss SER in the framework of COST P18 (Action C06.0114), as well as the Boninchi and Schmideiny Foundations. We gratefully acknowledge L. Bonacina for very fruitful discussions and M. Moret for his computational support.

[1] M. Hentschel, R. Kienberger, C. Spielmann, G. A. Reider, N. Milosevic, T. Brabec, P. Corkum, U. Heinzmann, M. Drescher, and F. Krausz, Nature (London) **414**, 509 (2001).
[2] A. Couairon, J. Biegert, C. Hauri, W. Kornelis, F. Helbing, U. Keller, and A. Mysyrowicz, J. Mod. Opt. **53**, 75 (2006).
[3] T. Fuji, T. Horio, and T. Suzuki, Opt. Lett. **32**, 2481 (2007).
[4] A. Zair, A. Guandalini, F. Schapper, M. Holler, J. Biegert, L. Gallmann, A. Couairon, M. Franco, A. Mysyrowicz, and U. Keller, Opt. Express **15**, 5394 (2007).
[5] S. Trushin, K. Kosma, W. Fuss, and E. Schmid, Opt. Lett. **32**, 2432 (2007).
[6] L. Bergé, S. Skupin, R. Nuter, J. Kasparian, and J.-P. Wolf, Rep. Prog. Phys. **70**, 1633 (2007).
[7] J. Kasparian and J.-P. Wolf, Opt. Express **16**, 466 (2008).
[8] A. Couairon and A. Mysyrowicz, Phys. Rep. **441**, 47 (2007).
[9] J. Kasparian *et al.*, Science **301**, 61 (2003).
[10] A. Mysyrowicz, A. Couairon, and U. Keller, New J. Phys. **10**, 025023 (2008).
[11] C. Hauri, W. Kornelis, F. Helbing, A. Heinrich, A. Couairon, A. Mysyrowicz, J. Biegert, and U. Keller, Appl. Phys. B: Lasers Opt. **79**, 673 (2004).
[12] L. Berge and S. Skupin, Phys. Rev. Lett. **100**, 113902 (2008).
[13] E. Matsubara, K. Yamane, T. Sekikawa, and M. Yamashita, J. Opt. Soc. Am. B **24**, 985 (2007).
[14] N. Karasawa, R. Morita, H. Shigekawa, and M. Yamashita, Opt. Lett. **25**, 183 (2000).
[15] Y. Zheng *et al.*, Opt. Lett. **33**, 233 (2008).
[16] T. Fuji and T. Suzuki, Opt. Lett. **32**, 3330 (2007).
[17] T. Pfeifer, M. Gallmann, M. Abel, D. Neumark, and S. Leone, Opt. Lett. **31**, 975 (2006).
[18] Z. Zeng, Y. Cheng, X. Song, R. Li, and Z. Xu, Phys. Rev. Lett. **98**, 203901 (2007).
[19] S. Zamith, Y. Ni, A. Gurtler, L. Noordam, H. Muller, and M. Vrakking, Opt. Lett. **29**, 2303 (2004).
[20] C. M. Kim, I. J. Kim, and C. H. Nam, Phys. Rev. A **72**, 033817 (2005).
[21] Y. Oishi, M. Kaku, A. Suda, F. Kannari, and K. Midorikawa, Opt. Express **14**, 7230 (2006).
[22] H. Mashiko, S. Gilbertson, C. Li, S. D. Khan, M. M. Shakya, E. Moon, and Z. Chang, Phys. Rev. Lett. **100**, 103906 (2008).
[23] M. Kolesik and J. V. Moloney, Phys. Rev. E **70**, 036604 (2004).
[24] L. Bergé, S. Skupin, G. Mejean, J. Kasparian, J. Yu, S. Frey, E. Salmon, and J. P. Wolf, Phys. Rev. E **71**, 016602 (2005).
[25] P. Bejot, J. Kasparian, and J.-P. Wolf, Opt. Express **16**, 14115 (2008).
[26] W. Press, B. Flannery, S. Teukolsky, and W. Vetterling, *Numerical Recipies* (Cambridge University Press, Cambridge, U.K., 1989).
[27] P. Béjot, C. Bonnet, V. Boutou, and J.-P. Wolf, Opt. Express **15**, 13295 (2007).
[28] F. Courvoisier, V. Boutou, J. Kasparian, E. Salmon, G. Mejean, J. Yu, and J. P. Wolf, Appl. Phys. Lett. **83**, 213 (2003).
[29] G. Mejean *et al.*, Phys. Rev. E **72**, 026611 (2005).
[30] A. Cavalieri *et al.*, Nature (London) **449**, 1029 (2007).